Journal of Polymer Research (2021) 28:219
https://doi.org/10.1007/s10965-021-02579-x

ORIGINAL PAPER

Porous organic/inorganic polymers based on double-decker silsesquioxane for high-performance energy storage

Mohamed Gamal Mohamed[1] · Wei-Cheng Chen[1] · Ahmed F. M. EL-Mahdy[1] · Shiao-Wei Kuo[1,2]

Received: 21 April 2021 / Accepted: 18 May 2021

Abstract

Two porous organic/inorganic microporous polymers (TPE-DDSQ POIP and Car-DDSQ POIP) were prepared through the Sonogashira-Hagihara coupling reaction of DDSQBr with 1,1,2,2-tetrakis(4-ethynylphenyl)ethene (TPE-T), and 3,3´,6,6´-tetraethynyl-9,9´-bicarbazole (Car-T); respectively. The chemical structure and properties of these two materials including thermal stability, porosity, crystallinity, and morphology were characterized in detail by using various instruments. Based on TGA analyses, Car-DDSQ POIP exhibited high thermal degradation temperature up to 439 °C and char yield up to 77.4 wt.% because inorganic DDSQ unit could enhance the thermal stability as expected. The electrochemical results revealed that TPE-DDSQ POIP and Car-DDSQ POIP showed specific capacitance of 22 and 23 F g^{-1} at 1 A g^{-1}; respectively in a three-electrode with KOH solution (6 M) as electrolyte and capacitance retention at about 93% after 2000 galvanostatic charge–discharge cycles.

Keywords Double-decker silsesquioxane · Conjugated microporous polymers · Energy storage

Introduction

Supercapacitors have been become an interesting topic in the industry and academic fields because of their unique characteristics such as excellent cycling stability, high durability, rapid charge–discharge process, low maintenance cost, and high-power density [1–10]. Supercapacitors can be considered as an important new sustainable device to reduce environmental pollution and energy crisis [11–20]. The supercapacitor mechanisms are divided into double-layer capacitance and pseudocapacitance. As known, most carbon materials were already used for double-layer capacitance such as templated porous carbons, activated carbon, graphite oxide, carbon nanotubes, and carbon aerogels [21–28]. Nowadays, the using pseudocapacitors devices are more than double-layer capacitance because their unique features such as possess reversible redox reactions on the electrode surface, and they can store charges in the double layer [29–39]. Metal oxides/hydroxides materials, covalent organic polymers (COPs), metal–organic framework (MOF), and conducting polymers could be applied in pseudocapacitance [37–39]. Porous organic polymers (POPs) are considered as emerging materials due to their tunable porosity, post-functionalization modifications, good thermal stability, chemical resistance, and optoelectronic properties [40–50]. The POPs have applied in various potential applications including power storage devices, separation analysis, optoelectronic, heterogenous catalysis, light-harvesting, oxygen reduction reaction, drug delivery, gas adsorption, water treatment, hydrogen evolution (H_2), lithium, potassium, and sodium-ion batteries, chemosensing and so on [51–60]. The preparation of POPs could be achieved through different kinds of methods including Sonogashira-Hagihara, Yamamoto coupling, Suzuki coupling, Buchwald–Hartwig (BH) coupling, chemical oxidative polymerization, Heck and Schiff-base condensation reactions [61–67].

Inorganic polyhedral oligomeric silsesquioxane (POSS) is considered as smallest silica nanostructured material with a diameter in the range 1–3 nm and has numerical formula $(RSiO_{1.5})_n$. The CMPs properties (such as flame water resistance, mechanical, chemical, and thermal stabilities) could be significantly improved through the incorporation of rigid POSS moieties in their polymeric framework [68–75].

✉ Shiao-Wei Kuo
kuosw@faculty.nsysu.edu.tw

[1] Department of Materials and Optoelectronic Science, National Sun Yat-Sen University, Kaohsiung 804, Taiwan

[2] Department of Medicinal and Applied Chemistry, Kaohsiung Medical University, Kaohsiung 807, Taiwan

Published online: 21 May 2021

As reported, the synthesis of CMPs materials containing bulky POSS nanocomposite unit could be achieved by Heck, Suzuki, and Sonogashira-Hagihara coupling reaction [76–82]. Double-decker–shaped polyhedral silsesquioxanes (DDSQ) are considered a type of biofunctionalized POSS derivatives and DDSQ molecule has been used to produce polymer/POSS nanocomposites including polyimide and polyurethane. As expected, the incorporation DDSQs into the polymeric framework can be enhanced the thermal properties of the materials due to it is bulky and hollow structures [72, 73]. Bicarbazole molecule is heterocyclic and nonplanar compounds with full aromaticity and large dihedral angles at around 70° [12, 83, 84]. Bicarbazole compound is easily prepared through the oxidation of carbazole derivatives by $KMnO_4$ and bicarbazole moiety has been applied in OLEDs and energy storage applications [12, 83, 84].

We have successfully prepared mesoporous poly(cyanate ester)–functionalized DDSQ and these framework materials having good thermal stability and a specific capacitance of 20 F g^{-1} at 5 mV s^{-1} [85]. To the best of our knowledge, this is the first report for the preparation of POIPs containing DDSQ, tetraphenylethene, and bicarbazole moieties and investigates their properties. Herein, by considering the interesting properties of POPs and DDSQ molecule, two POIPs- TPE-DDSQ POIP and Car-DDSQ POIP were prepared successfully through the Sonogashira-Hagihara coupling reaction of brominated DDSQ as a building unit with 1,1,2,2-tetrakis(4-ethynylphenyl)ethene (TPE-T), and 3,3´,6,6´-tetraethynyl-9,9´-bicarbazole (Car-T), as displayed in Scheme 1. The surface morphologies, thermal stability, chemical structure, and porosity properties of TPE-DDSQ POIP and Car-DDSQ POIP were investigated in detail by using different instruments. As expected, both these two POIPs materials displayed high decompositions temperature up to 400 °C and char yield up to 70 wt.%, based on TGA results. Finally, according to the electrochemical results, we revealed that the TPE-DDSQ POIP and Car-DDSQ POIP showed high specific capacitance of 22 and 23 F g^{-1} at 1 A g^{-1} compared with other porous materials.

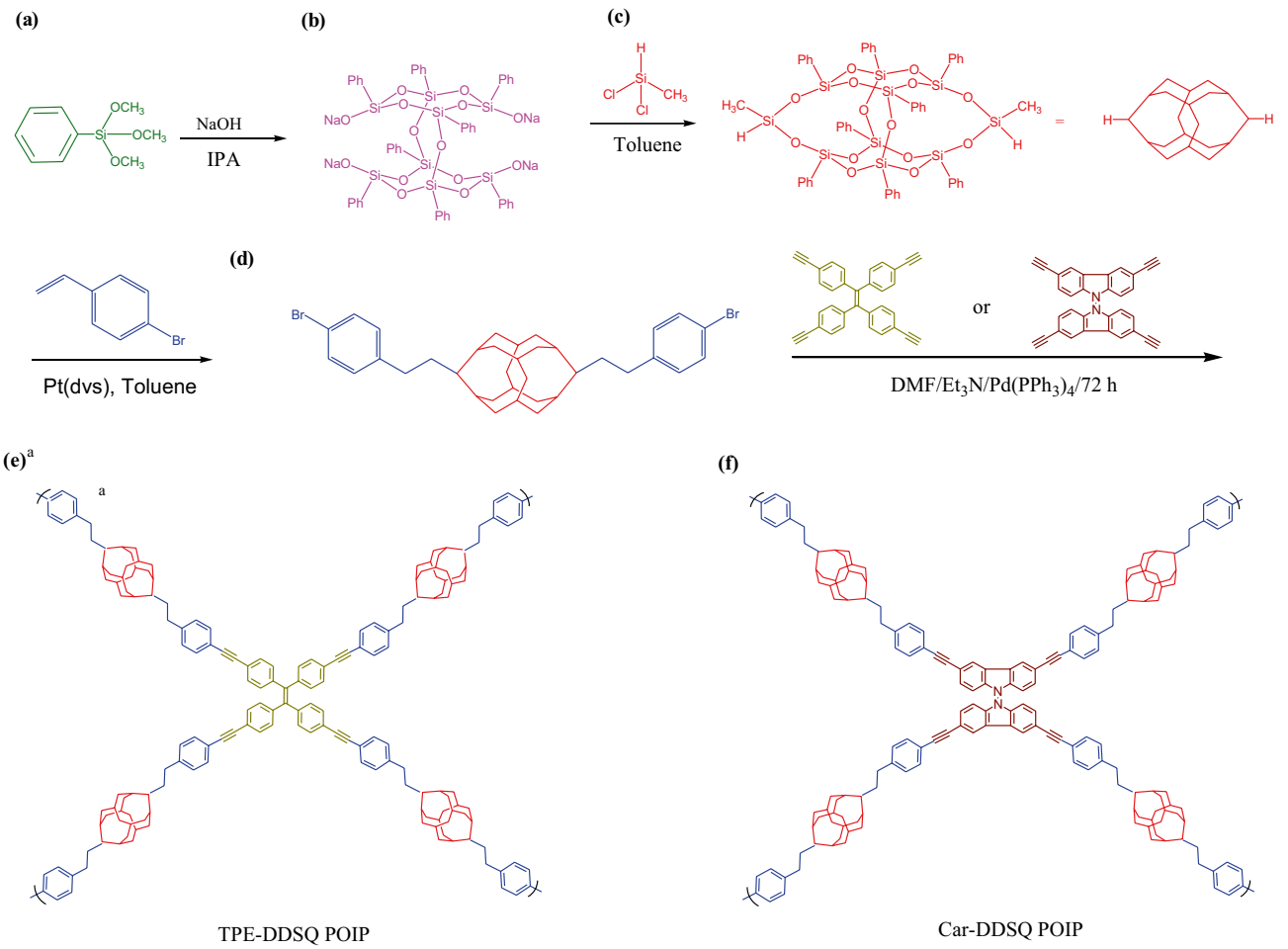

Scheme 1 Preparation of (**b**) DDNA (**c**) DDSQ (**d**) DDSQBr (**e**) TPE-DDSQ POIP and (**f**) Car-DDSQ POIP from (**a**) phenyltrimethoxylsilane

Experimental

Materials

Methyldichlorosilane, phenyltrimethoxylsilane, sodium hydroxide (NaOH), platinum divinyltetramethyldisiloxane complex [Pt(dvs)], tetrahydrofuran (THF), magnesium sulfate ($MgSO_4$), 2- propanol, and charcoal were purchased from Alfa-Aesar. Methanol (MeOH), ethanol (EtOH), sodium carbonate (K_2CO_3), ethyl acetate, were purchased from Sigma-Aldrich. Et_3N, CuI, triphenylphosphine (PPh_3), and $Pd(PPh_3)_4$ were purchased from Sigma–Aldrich. DMF was purchased from Acros. Double-decker silsesquioxane-Na (DD-Na), double-decker silsesquioxane (DDSQ), 3,3´,6,6´-tetrabromo-9,9´-bicarbazole (Car-Br_4), and tetrakis(4-bromophenyl)ethylene (TPE-Br_4) were synthesized at our lab [12, 25, 72, 73]. The preparation of 1,1,2,2-Tetrakis(4-((trimethylsilyl)ethynyl) phenyl)ethane (TPE-TMS) and 3,3´,6,6´-Tetrakis((trimethylsilyl)ethynyl)-9,9´-bicarbazole (Car-TMS) were provided in detail in the supporting information (Schemes S1 and S2, Figs. S1-S6).

Synthesis of DDSQBr

DDSQ (1 g, 0.87 mmol) and 4-bromostyrene (0.32 g, 0.23 mL, 1.75 mmol) were dissolved in 30 mL of toluene. After the refluxing, the reaction mixture at 50 °C for 1 h, few drops of Pt(dvs) were added, followed by refluxing at 90 °C for 2 days. Then, charcoal was added to the resulting mixture to remove the catalyst and the filtrate was concentrated. After that, the obtained white solid was washed with EtOH to give DDSQBr (0.80 g, 60.74%). ^{1}H NMR (500 MHz, $CDCl_3$, δ, ppm,): 7.52–6.9 (Ar–H), 2.67 (4H, $ArCH_2CH_2$), 1.52 (4H, $Si(CH_3)$ CH_2CH_2Ar).

1,1,2,2-Tetrakis(4-ethynylphenyl)ethene (TPE-T)

50 mL of anhydrous methanol was added into a mixture of K_2CO_3 (2.04 g, 14.82 mmol) and TPE-TMS (1.00 g, 1.47 mmol). After stirring for 24 h, the solution was poured into 200 mL of water to remove the excess amount of base to afford a pale-yellow precipitate (0.80 g, 93%). FTIR (KBr, cm^{-1}, Fig. S7): 3273 (≡C–H), 2109 (C≡C stretching). ^{1}H NMR (500 MHz, $CDCl_3$, δ, ppm, Fig. S8): 7.24 (d, 8H), 6.93 (d, 8H), 3.06 (s, 4H, ≡C–H). ^{13}C NMR (125 MHz, $CDCl_3$, δ, ppm, Fig. S9): 143.8, 141.6, 132.36, 132, 121.24, 83.6 (≡C–Ar), 77.88 (≡C–H). (T_{d5}: 252.18 °C, char yield: 70.73%, Fig. S10).

3,3´,6,6´-Tetraethynyl-9,9´-bicarbazole (Car-T)

50 mL of anhydrous methanol was added into Car-TMS (0.440 g, 0.650 mmol) and K_2CO_3 (0.900 g, 6.52 mmol). After stirring for 24 h, the solution was poured into 200 mL of water to afford a pale-yellow precipitate (0.35 g, 80%).

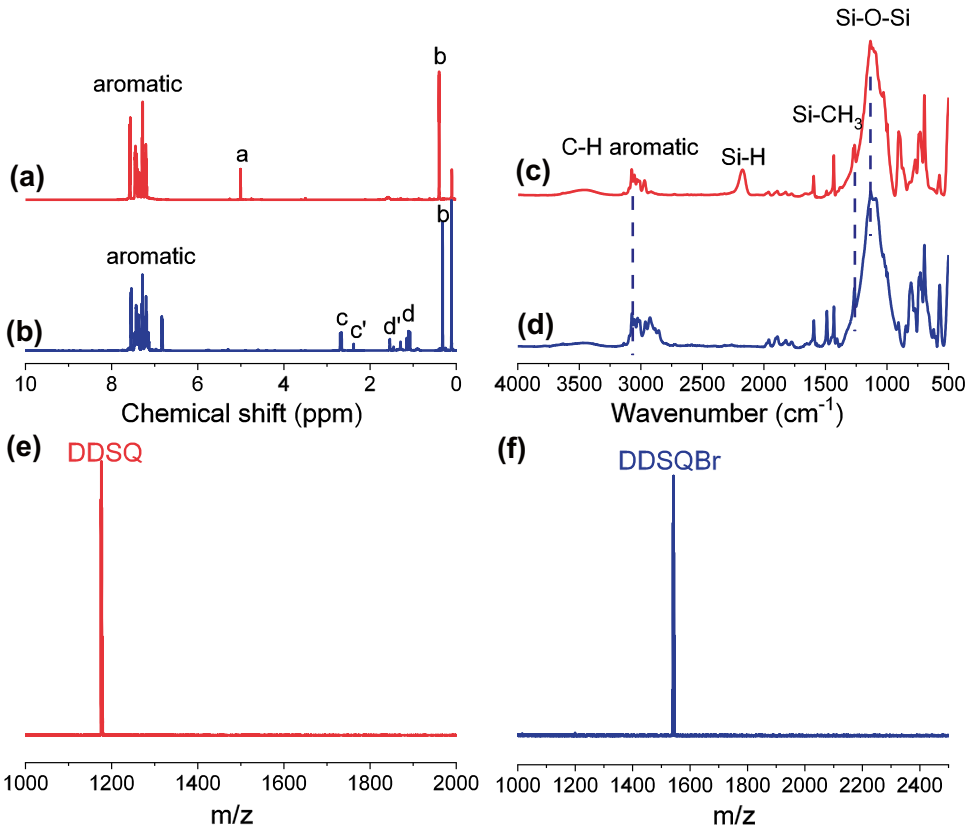

Fig. 1 ^{1}H NMR spectra of (**a**) DDSQ and (**b**) DDSQBr. FTIR profile of (**c**) DDSQ and (**d**) DDSQBr. MALDI-TOF mass spectra of (e) DDSQ and (**d**) DDSQBr

FTIR (KBr, cm^{-1}, Fig. S11): 3285 (≡C–H), 2105 (C≡C stretching). ^{1}H NMR (500 MHz, $CDCl_3$, δ, ppm, Fig. S12): 8.32 (s, 4H), 7.51 (d, 4H), 6.84 (d, 4H), 3.09 (s, 4H, ≡C–H). ^{13}C NMR (125 MHz, $CDCl_3$, δ, ppm, Fig. S13): 140.24, 132.02, 125.61, 122.24, 116.61, 109.77, 84.33 (≡C–Ar), 76.67 (≡C–H). (T_{d5}: 237 °C, char yield: 79.4%, Fig. S14).

Synthesis of TPE-DDSQ POIP and Car-DDSQ POIP

TPE-T or Car-T (100 g, 0.234 mmol), DDSQBr (710 mg, 0.470 mmol), CuI (3.2 mg, 0.0170 mmol), PPh_3 (4.40 mg, 0.0170 mmol), and $Pd(PPh_3)_4$ (19.20 mg, 0.0166 mmol) were dissolved in DMF (5 mL) and Et_3N (5 mL) was heated under reflux at 100 °C for 3 days in a Pyrex tube to afford TPE-DDSQ POIP as a green powder (0.08 g, 80%) and Car-DDSQ POIP as a yellow powder (0.07 g, 70%).

Results and discussion

Synthesis of DDSQBr, TPE-DDSQ POIP, and Car-DDSQ POIP

Scheme 1 shows our synthetic method to prepare two different kinds of conjugated microporous polymers based on DDSQ nanocomposites. Firstly, DDSQ was prepared from the reaction of double-decker silsesquioxane-Na (DD-Na) with methyldichlorosilane in the presence of triethylamine as a base in THF as solvent [Scheme 1(b)]. Secondly, the brominated DDSQ (DDSQBr) was synthesized through the hydrosilylation reaction of DDSQ with 4-bromostyrene in the presence of Pt(dvs) as a catalyst and toluene as solvent at 90 °C for 48 h Scheme 1(c). Thirdly, two new TPE-DDSQ POIP and Car-DDSQ POIP were synthesized through the Sonogashira-Hagihara coupling reaction based on DDSQBr with TPE-T, and Car-T as shown in Scheme 1(d) and 1(e).

The chemical structures of DDSQ and DDSQBr were confirmed by FTIR, ^{1}H-NMR and MALDI-TOF measurements. Figures 1(a) and (b) display the ^{1}H-NMR spectra of DDSQ and DDSQBr in $CDCl_3$, recorded at room temperature. The proton signals of DDSQ appeared at 4.99 (peak a), 0.36 (peak b), and 7.54–7.18 ppm which are assigned to Si–H, Si-CH_3, and aromatic protons: respectively Fig. 1(a) [72, 73]. The ^{1}H-NMR spectrum of DDSQBr (Fig. 1(a)) shows the signals at 1.52, 2.67, and 7.52–6.90 ppm corresponding to $SiCH_2CH_2$, $ArCH_2CH_2$, and aromatic protons, respectively. In addition, the disappearance signals at 4.99 ppm for the Si–H unit in the ^{1}H-NMR spectrum of DDSQBr, indicating the complete hydrosilylation reaction of DDSQ with 4-bromostyrene and formation of DDSQBr in high purity. The characteristics absorption bands of DDSQ and located at 3075, 1260, and 1136 cm^{-1}, which are attributed to the stretching CH aromatic, $Si-CH_3$, and Si–O-Si units, as displayed in Fig. 1(c) and (d). The absorption band of the $Si-H$ stretching was completely disappeared in the FTIR spectrum of DDSQBr (Fig. 1(d)) after

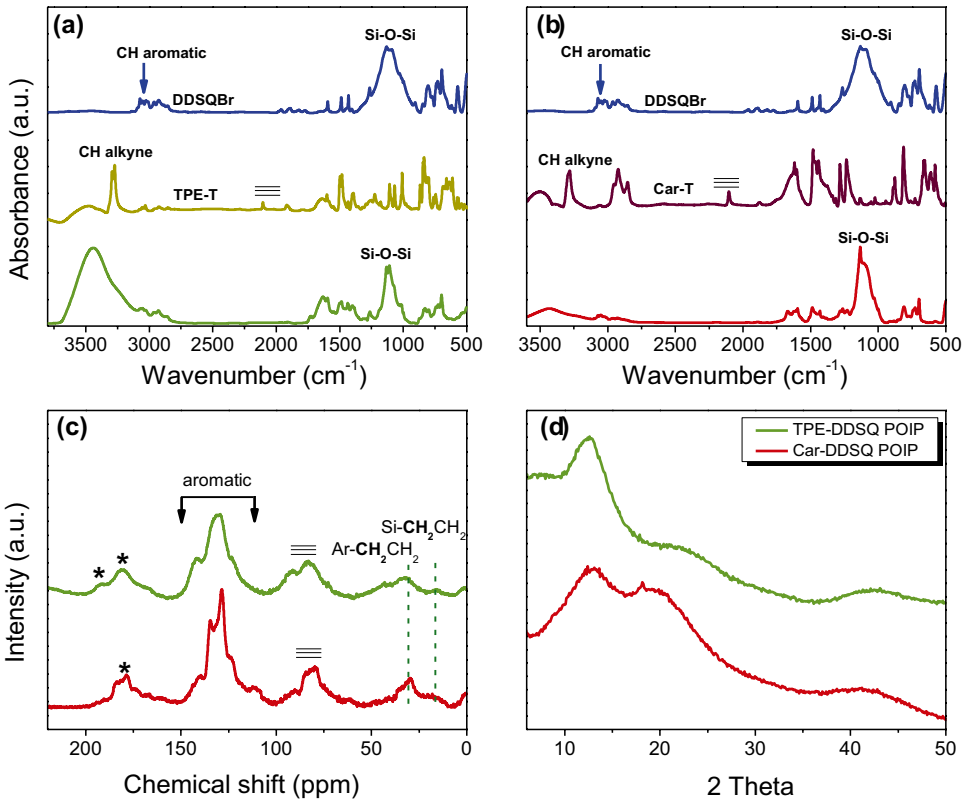

Fig. 2 (**a**) and (**b**) FTIR analyses of DDSQBr, TPE-T, Car-T, TPE-DDSQ POIP, and Car-DDSQ CMP. (**c**) and (**d**) Solid-state ^{13}C NMR and XRD spectra of TPE-DDSQ POIP and Car-DDSQ POIP

the hydrosilylation and transformation reactions. Furthermore, the molecular structures of DDSQ and DDSQBr were also confirmed via MALDI-TOF mass spectrometry measurements as shown in Fig. 1(e) and (f). Both DDSQ and DDSQBr mass spectra feature one signal centered at 1176 and 1546 g/mol for $[DDSQ + Na]^+$ and $[DDSQBr + Na]^+$; respectively. Mass spectral, NMR, and FTIR confirmed the successful preparation of the new DDSQBr monomer.

To confirm the formation and successful synthesis of our new TPE-DDSQ POIP and Car-DDSQ POIP, the FTIR and solid-state NMR analyses were performed as shown in Fig. 2. As presented in the FTIR profile (Fig. 2), the characteristic absorption bands of DDSQBr (Figs. 1(d) and 2(a)) are located at 3075, 1260, and 1136 cm^{-1} for the aromatic CH stretching, Si-CH_3 stretching, and the Si–O-Si unit. The FTIR spectrum of TPE-T (Fig. 2(a)) showed the peaks for the alkynyl C-H stretching, and–C≡C–stretching at 3275 and 2097 cm^{-1}, respectively. In addition, the FTIR spectrum of Car-T (Fig. 2(b)) showed a strong and weak absorption band at 3279 and 2099 cm^{-1}, corresponding to alkynyl C-H stretching, and –C≡C– stretching. Both FTIR spectrum of TPE-DDSQ POIP and Car-DDSQ POIP (Fig. 2(a) and (b)) displayed the absorption signals centered at 3445, 1261, and 1133 cm^{-1}, respectively, representing to absorbed water, Si-CH_3 and Si–O-Si units. we observed that the disappearance absorption band for alkynyl C-H stretching in the FTIR spectra of TPE-DDSQ POIP and Car-DDSQ POIP, indicating that successful and complete the Sonogashira-Hagihara coupling of DDSQBr with TPE-T, and Car-T; respectively. The solid-state ^{13}C NMR spectra of TPE-DDSQ POIP and Car-DDSQ POIP (Fig. 2(c)) revealed signals located in the ranges 141.82–122.77 and 140.15–123.26 ppm for TPE-DDSQ POIP and Car-DDSQ POIP respectively, corresponding to the carbon resonance of the aromatic units. In addition, the carbon nuclei of the internal alkynyl bonds, Ar$\mathbf{CH_2}CH_2$ and Si$\mathbf{CH_2}CH_2$ units appeared at 83.38, 31.72, and 16.59 ppm, respectively in both TPE-DDSQ CMP and Car-DDSQ POIP polymeric framework. The XRD analyses (Fig. 2(d)) displayed that the TPE-DDSQ POIP and Car-DDSQ POIP had amorphous properties and no possess any crystalline peaks.

Thermal degradation temperatures (T_{d5} and T_{d10}) and char yield were 318 °C, 406 °C, and 71.4 wt.%; respectively, for TPE-DDSQ POIP and 290 °C, 439 °C and 77.4 wt.%; respectively for Car-DDSQ POIP, based on TGA analyses (Fig. 3and Table S1). In addition, the continuous weight loss starting from relatively low temperatures for TPE-DDSQ POIP and Car-DDSQ POIP framework due to the aliphatic CH_2-CH_2 units as a flexible group in the DDSQ moiety. Furthermore, both materials showed excellent thermal stability up to 400 °C.

To scrutinize the porosity properties and BET specific surface areas of TPE-DDSQ POIP and Car-DDSQ POIP, N_2 adsorption/desorption measurements were done at 77 K, as displayed in Fig. 4. As shown in Fig. 4(a) and (b), the N_2 adsorption/desorption curves of TPE-DDSQ

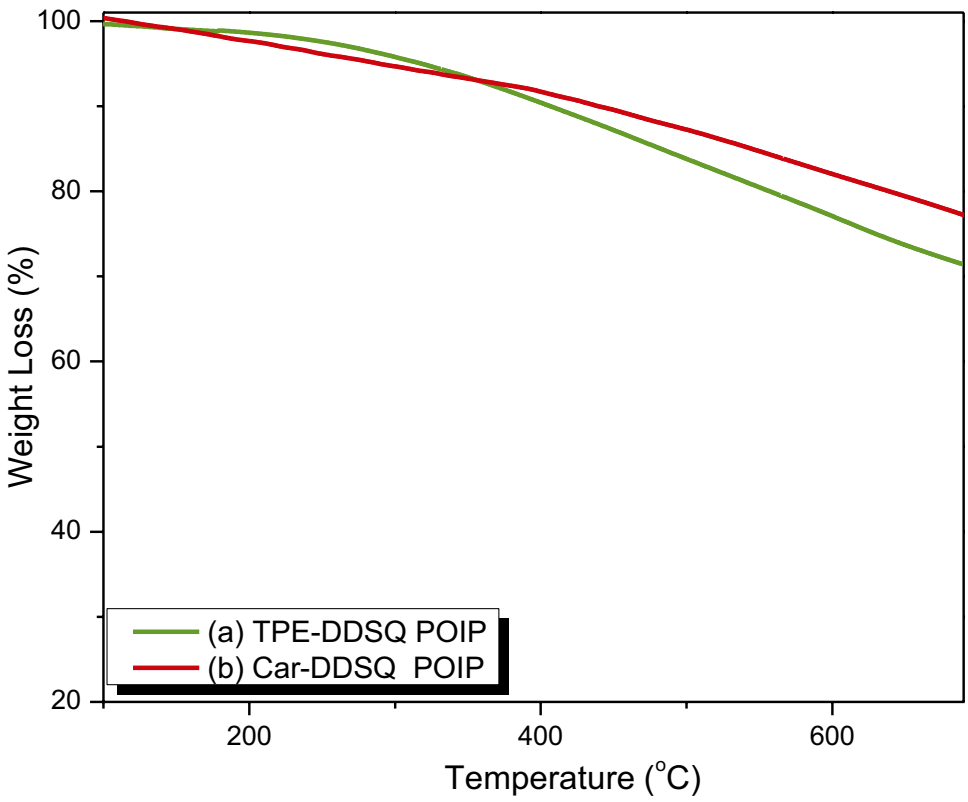

Fig. 3 TGA analyses of (**a**) TPE-DDSQ POIP and (**b**) Car-DDSQ POIP

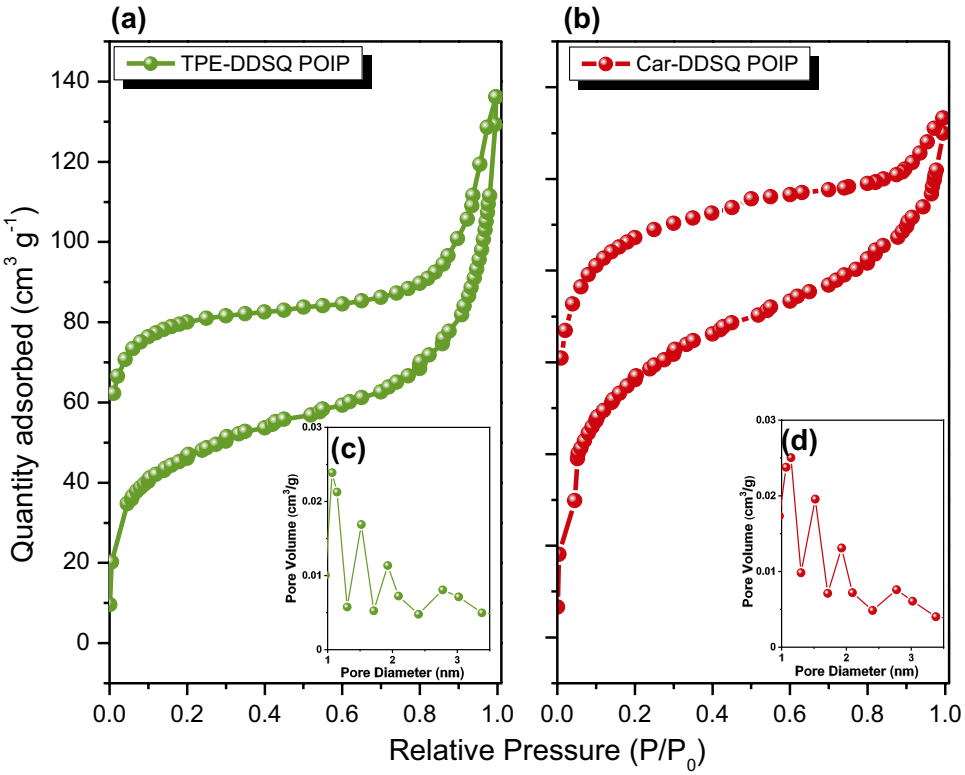

Fig. 4 N_2 adsorption/desorption and pore size distribution of TPE-DDSQ POIP (**a**, **c**) and Car-DDSQ POIP curves (**b**, **d**)

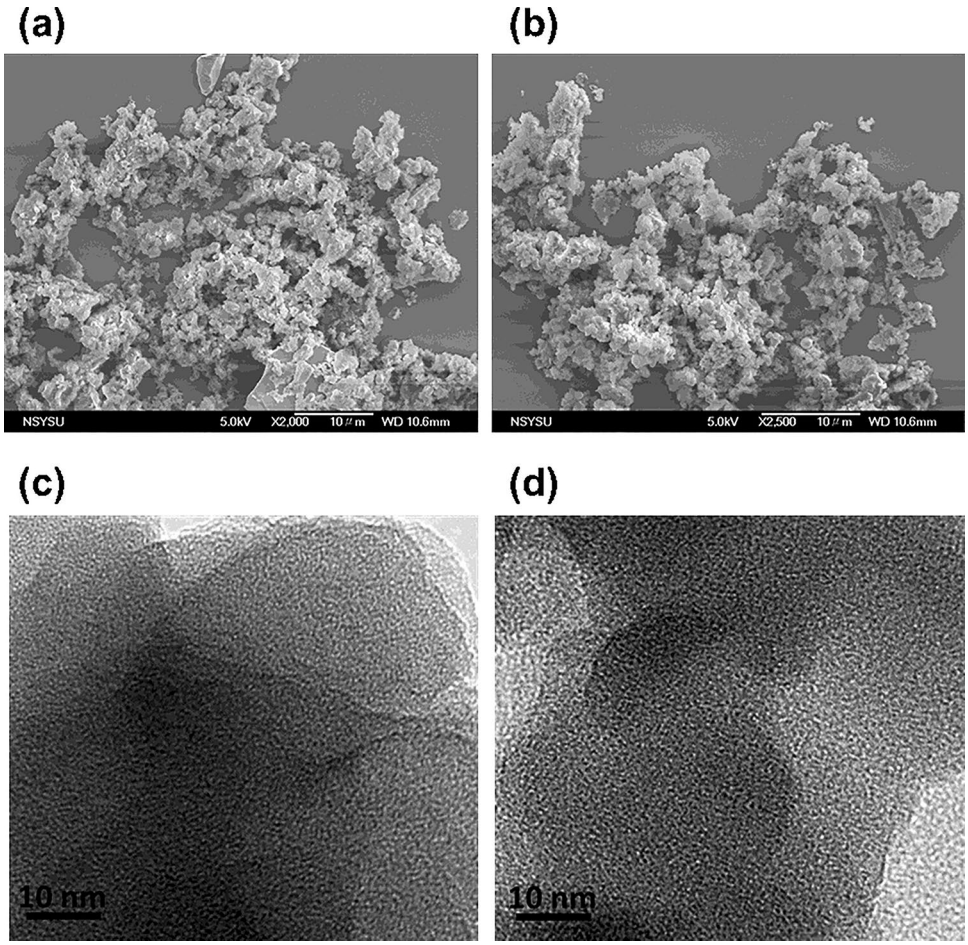

Fig. 5 SEM and TEM images of TPE-DDSQ POIP (**a**, **c**) and Car-DDSQ POIP curves (**b**, **d**)

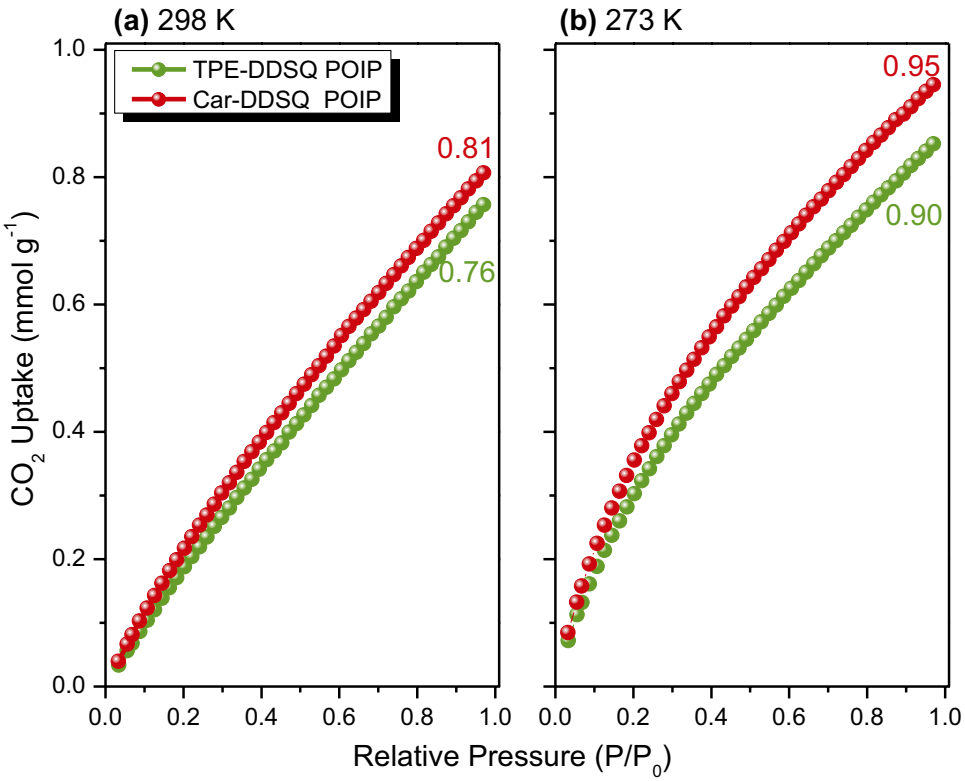

Fig. 6 CO_2 uptake of (**a**) TPE-DDSQ POIP and (**b**) Car-DDSQ POIP

POIP and Car-DDSQ POIP features type I and IV with BET specific surface area and total pore volume of 157.67 $m^2\ g^{-1}$, 0.20 $cm^3\ g^{-1}$, and 256.34 $m^2\ g^{-1}$, 0.25 $cm^3\ g^{-1}$; respectively. Also, the N_2 adsorption/desorption profiles of the TPE-DDSQ POIP and Car-DDSQ POIP showed the high N_2 uptake at low and high pressure, indicating the presence of micro and mesoporous inside their polymeric framework. We observed that the hysteresis loop of N_2 adsorption/desorption curves of TPE-DDSQ POIP and Car-DDSQ POIP (Fig. 4(a) and (b)) does not close completely during the gas adsoprtion process because of the presence of POSS as a flexibility structure inside the polymeric framework of these materials by elastic deformations. The pore size distribution of these two materials was investigated by using the non-local density functional theory (NLDFT) model, as shown in Fig. 4(c) and (d). The results revealed that the pore size distribution of the TPE-DDSQ POIP was in the ranges 1.06–2.76 nm. While the pore size distribution of the Car-DDSQ POIP was in the ranges 1.14–2.78 nm.

The surface morphologies were examined through SEM and TEM measurements for TPE-DDSQ POIP and Car-DDSQ POIP, as seen in Fig. 5(a) and (b). The SEM images [Fig. 5(a) and (b)] revealed that interconnected aggregated small spheres in these materials. Furthermore, TEM analyses showed that these materials feature amorphous properties which consistent with XRD analyses and microporous structure [Fig. 5(c) and (d)].

The improvement of CO_2 uptake performance of the porous polymers strongly depends on permanent porosity, high BET surface area, and incorporation of some polar groups (such as COOH, -OH, $-NH_2$) in their framework structure [12, 14, 31, 86–88]. Thus, the CO_2 uptake performance of TPE-DDSQ POIP and Car-DDSQ POIP (Fig. 6(a) and (b)) was checked through the CO_2 isotherm analyses, recorded at two different temperatures (298 and 273 K). From Fig. 6, The values of CO_2 adsorption capacity reached to be 0.76 and 0.90 mmol g^{-1} for TPE-DDSQ POIP at 298 and 273 K; respectively. While the values of CO_2 uptake of Car-DDSQ POIP were found to be 0.81 mmol g^{-1} at 298 and 0.95 mmol g^{-1} at 273 K. The results showed that Car-DDSQ POIP possesses good CO_2 uptake compared to TPE-DDSQ POIP which is assigned to its high S_{BET} surface area and the presence of N atoms in the bicarbazole units, which could enhance the interaction with CO_2 molecules.

Electrochemical performance of TPE-DDSQ POIP and Car-DDSQ POIP

The electrochemical properties of the TPE-DDSQ POIP and Car-DDSQ POIP porous materials were tested through cyclic voltammetry (CV) and galvanostatic charge–discharge (GCD) analyses. Fig. 7(a) and (b) show the cyclic voltammetry (CV) profiles at different scan rates from 5 to 200 mV s^{-1} within the potential window of -0.6 V to 0.2 V and -0.8 V to 0.4 V versus Hg/HgO for TPE-DDSQ

POIP and Car-DDSQ POIP, respectively. The resulting CV curve of the Car-DDSQ POIP (Fig. 7(b)) showed two redox peaks can be seen at all scan rates, which indicated that this material had pseudocapacitance and pseudopotential character. Interestingly, redox peaks of the Car-DDSQ POIP were kept even with increasing the scan rate from 10 to 100 mV s^{-1}. When the scan rate was 200 mV s^{-1}, the redox peak currents were still observed at -0.25 V and 0.004 V; respectively, and CV curve areas increased, indicating that the Car-DDSQ POIP possess excellent capacitance performance at all potential scan rate. On contrary, in the CV curve of the TPE-DDSQ POIP (Fig. 7(a)) can be observed irreversible redox peak that corresponds to the double bond in the TPE unit, demonstrating that this material had capacitance character. The GCD curves of the TPE-DDSQ POIP and Car-DDSQ POIP at different current densities are presented in Fig. 7(c) and (d). The GCD profiles of the TPE-DDSQ POIP and Car-DDSQ POIP possessed triangular shapes with a slight bend. In addition, the GCD curve of Car-DDSQ POIP exhibited longer discharging times compared to the TPE-DDSQ POIP due to the presence of a carbazole unit within the Car-DDSQ POIP framework. Therefore, Car-DDSQ POIP had EDLC and pseudocapacity characteristics. The maximum specific capacitance of the TPE-DDSQ POIP and Car-DDSQ POIP (Fig. 8(a)) was determined through GCD curves to be 22 and 23 F g^{-1}; respectively at 1 A g^{-1}. Dichtel et al. revealed that TAAQ-TFP-COF displaying a specific capacitance of 48 F g^{-1} at 0.2 A g^{-1} [89]. In 2020, Mohamed et al. observed that hypercrosslinked polymers containing tetraphenylanthraquinone unit (An-CPOP-2) having a specific capacitance of 98.4 F g^{-1} [90]. Furthermore, our COF materials based on electrodes such as Car-TPA-COF, Car-TPP-COF, Car-TPT COF, TPA-COF-1, TPA-COF-2, TPA-COF-3, TPT-COF-4, TPT-COF-5, and TPT-COF-6 possess.

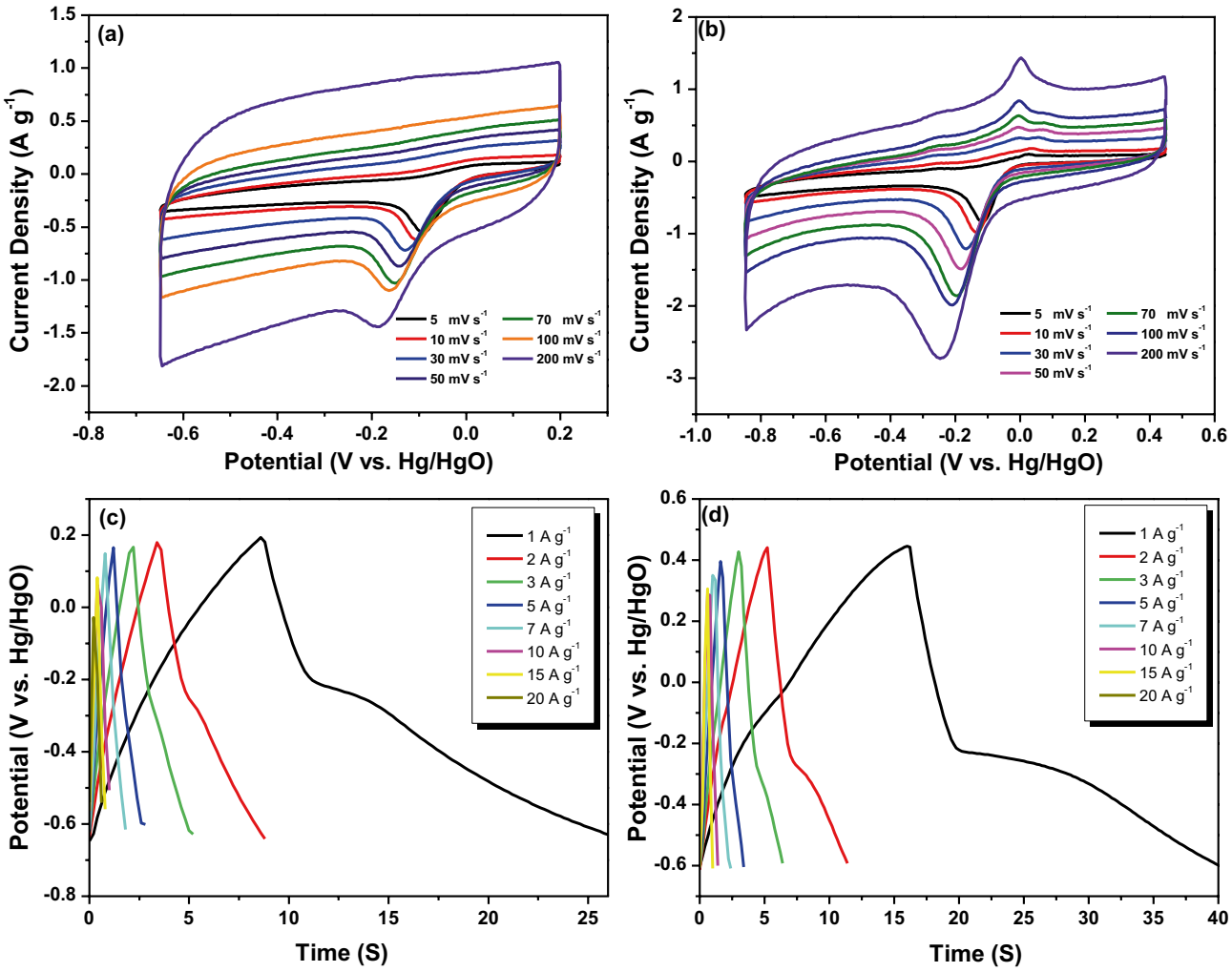

Fig. 7 CV profiles of (**a**) TPE-DDSQ POIP and (**b**) Car-DDSQ POIP. GCD curves of (**c**) TPE-DDSQ POIP and (**d**) Car-DDSQ POIP, recorded at a different current density from 1 to 20 A g^{-1}

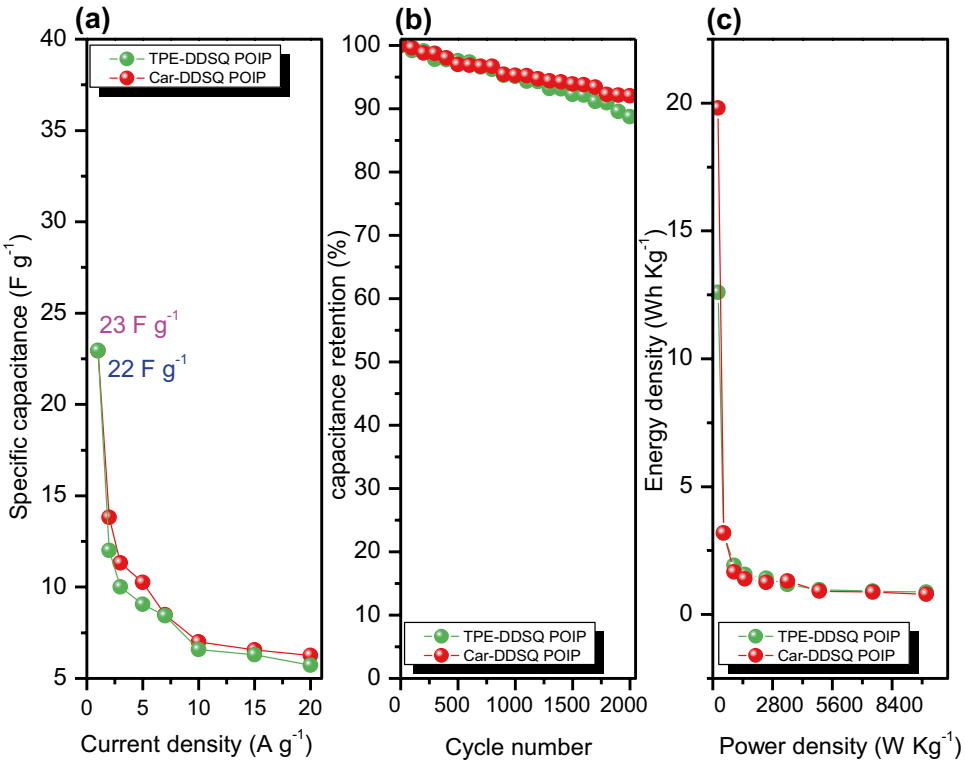

Fig. 8 (**a**) Specific capacitances performance of TPE-DDSQ POIP and Car-DDSQ POIP. (**b**) Cycling stabilities of TPE-DDSQ POIP and Car-DDSQ POIP, obtained at 10 A g^{-1} after 2000 cycles. (**c**) Ragone plot of TPE-DDSQ POIP and Car-DDSQ POIP

capacitance values of 13.6, 14.5, 17.4, 51.3, 14.4, 5.1, 2.4, 0.34, and 0.24 F g^{-1} [91]. The performance and stability of the TPE-DDSQ POIP and Car-DDSQ POIP (Fig. 8(b)) based as electrodes were tested through GCD measurement at 10 A g^{-1}. The results revealed that the capacitance retention rate of the TPE-DDSQ POIP and Car-DDSQ POIP was 89 and 93%; respectively after 2000 cycles. Furthermore, the energy and power densities of the Car-DDSQ POIP electrode were higher than that of the TPE-DDSQ POIP, due to its high S_{BET} surface area, and the presence of N atoms in the bicarbazole units, based on Ragone plots (Fig. 8(c)). In summary, the Car-DDSQ POIP electrode had a higher specific capacitance (23 F g^{-1}) and capacitance retention (93%) compared with other porous materials (Table S2), demonstrating that Car-DDSQ POIP could be acted as a pseudocapacitive electrode material.

Conclusions

To conclude, two kinds of porous organic/inorganic POIPs (TPE-DDSQ POIP and Car-DDSQ POIP) based on inorganic double-decker silsesquioxane, tetraphenylethene, and bicarbazole units have been successfully synthesized through the Sonogashira-Hagihara coupling reaction. In addition, these TPE-DDSQ POIP and Car-DDSQ POIP materials displayed outstanding thermal stability, according to TGA measurements because of inorganic DDSQ in POIP. Furthermore, a new Car-DDSQ POIP possessed a high specific capacitance of 23 F g^{-1} at 1 A g^{-1} and a good capacitance retention rate (93%) due to the presence of bicarbazole units, its S_{BET} surface area (256.34 m^2 g^{-1}), and large pore size (1.14–2.78 nm). Thus the Car-DDSQ POIP could be acted as a pseudocapacitive electrode material.

Supplementary Information The online version contains supplementary material available at https://doi.org/10.1007/s10965-021-02579-x.

Acknowledgements This study was supported financially by the Ministry of Science and Technology, Taiwan, under contracts MOST 108-2638-E-002-003-MY2, and 108-2221-E-110-014-MY3. The authors thank the staff at National Sun Yat-sen University for assistance with TEM (ID: EM022600) experiments.

Data availability Data not available / The authors do not have permission to share data.

Declarations

Conflict of interest There are no conflicts to declare.

References

1. Liao Y, Wang H, Zhu M, Thomas A (2018) Efficient supercapacitor energy storage using conjugated microporous polymer networks synthesized from buchwald-hartwig coupling. Adv Mater 30:1705710
2. Choudhary N, Li C, Moore J, Nagaiah N, Zhai L, Jung Y, Thomas J (2017) Asymmetric supercapacitor electrodes and devices. Adv Mater 29:1605336
3. Chen S, Ma W, Cheng Y, Weng Z, Sun B, Wang L, Chen W, Li F, Zhu M, Cheng H (2015) Scalable non-liquid-crystal spinning of locally aligned graphene fibers for high-performance wearable supercapacitors. Nano Energy 15:642–653
4. Hung WS, Ahmed MMM, Mohamed MG, Kuo SW (2020) Competing hydrogen bonding produces mesoporous/macroporous carbons templated by a high-molecular-weight poly(caprolactone–b–ethylene oxide–b–caprolactone) triblock copolymer. J Polym Res 27:173
5. Mohamed MG, Ahmed MMM, Du WT, Kuo SW (2021) Meso/Microporous Carbons from conjugated hyper-crosslinked polymers based on tetraphenylethene for high-performance CO_2 capture and supercapacitor. Molecules 26:738
6. Pal R, Goyal SL, Rawal I (2020) High-performance solid-state supercapacitors based on intrinsically conducting polyaniline/MWCNTs composite electrodes. J Polym Res 27:179
7. Vinodh R, Gopi CVVM, Kummara VGR, Atchudanc R, Ahamad T, Sambasivam S, Yi M, Obaidat IM, Kim HJ (2020) A review on porous carbon electrode material derived from hypercrosslinked polymers for supercapacitor applications. J Energy Storage 32:101831
8. Samy MM, Mohamed MG, Kuo SW (2020) Pyrene-functionalized tetraphenylethylene polybenzoxazine for dispersing single-walled carbon nanotubes and energy storage. Compos Sci Technol 199:108360
9. Quan T, Breteseché NG, E. Härk E, Kochovski Z, Mei S, Pinna N, Ballauff M, Lu Y (2019) Highly dispersible hexagonal Carbon–MoS_2–Carbon nanoplates with hollow sandwich structures for supercapacitors. Chem Eur J 25:4757–4766
10. Mohamed MG, Jr ECA, Matsagar BM, Na JB, Yamauchi Y, Wu KCW, Kuo SW (2020) Construction hierarchically mesoporous/microporous materials based on block copolymer and covalent organic framework. J Taiwan Inst Chem Eng 112:180–192
11. Torad NL, Salunkhe RR, Li Y, Hamoudi H, Imura M, Sakka Y, Hu CC, Yamauchi Y Electric double-layer capacitors based on highly graphitized nanoporous carbons derived from ZIF-67. Chem. Eur. J. 20:7895–7900.
12. Mohamed MG, EL-Mahdy AFM, Ahmed MMM, Kuo SW (2019) Direct synthesis of microporous bicarbazole-based covalent triazine frameworks for high-performance energy storage and carbon dioxide uptake. ChemPlusChem 84:1767–1774
13. Tang J, Wang T, Salunkhe RR, Alshehri SM, Malgras V, Yamauchi Y (2015) Three-dimensional nitrogen-doped hierarchical porous carbon as an electrode for high-performance supercapacitors. Chem Eur J 21:17293–17298
14. Mohamed MG, EL-Mahdy AFM, Takashi Y, Kuo SW (2020) Ultrastable conductive microporous covalent triazine frameworks based on pyrene moieties provide high-performance CO_2 uptake and supercapacitance. New J Chem 44:8241–8253
15. Li Y, Zheng S, Liu X, Li P, Sun L, Yang R, Wang S, Wu Z, Bao X, Deng WQ (2018) Conductive microporous covalent triazine-based framework for high-performance electrochemical capacitive energy storage. angew. Chem. Int Ed 57:7992–7996
16. Simon P, Gogotsi Y (2008) Materials for electrochemical capacitors. Nat Mater 7:845–854
17. Bhanja P, Das SK, Bhunia K, Pradhan D, Hayashi T, Hijikata Y, Irle S, Bhaumik A (2018) A new porous polymer for highly efficient capacitive energy storage. ACS Sustainable Chem Eng 6:202–209
18. Wu ZS, Parvez K, Feng X, Muellen K (2013) Graphene-based in-plane micro-supercapacitors with high power and energy densities. Nat Commun 4:2487
19. Liu Y, Hao X, Wang L, Xu Y, Liu J, Tian X, Yao B (2019) Facile synthesis of porous carbon materials with extra high nitrogen content for supercapacitor electrodes. New J Chem 43:3713–3718
20. EL-Mahdy AFM, Yu TC, Kuo SW (2021) Synthesis of multiple heteroatom–doped mesoporous carbon/silica composites for supercapacitors. Chem Eng J 414:128796
21. Wang G, Zhang L, Zhang J (2012) A review of electrode materials for electrochemical supercapacitors. Chem Soc Rev 41:797–828
22. Awata R, Shehab M, Tahan AE, Soliman M, Ebrahim S (2020) High performance supercapacitor based on camphor sulfonic acid doped polyaniline/multiwall carbon nanotubes nanocomposite. Electrochim Acta 347:136299
23. Zhai Z, Ren B, Zheng Y, Xu Y, Wang S, Zhang L, Liu Z (2019) Nitrogen-containing carbon aerogels with high specific surface area for supercapacitors. Chem Electro Chem 6:5993
24. Li P, Xie H, Liu Y, Wang J, Wang X, Xie Y, Hu W, Xie T, Wang Y, Zhang Y (2020) Dual-templated 3D nitrogen-enriched hierarchical porous carbon aerogels with interconnected carbon nanosheets from self-assembly natural biopolymer gel for supercapacitors. Electrochim Acta 353:136514
25. El-Mahdy AFM, Mohamed MG, Mansoure TH, Yu HH, Chen T, Kuo SW (2019) Ultrastable tetraphenyl-p-phenylenediamine-based covalent organic frameworks as platforms for high-performance electrochemical supercapacitors. Chem Commun 55:14890–14893
26. Zang X, Wang X, Liu H, Ma X, Wang W, Ji J, Chen J, Li R, Xue M (2020) Enhanced ion conduction via epitaxially polymerized two-dimensional conducting polymer for high-performance cathode in zinc-ion batteries. ACS Appl Mater Interfaces 12:9347–9354
27. Veerakumar P, Sangili A, Manavalan S, Thanasekaran P, Lin KC (2020) Research progress on porous carbon supported metal/metal oxide nanomaterials for supercapacitor electrode applications. Ind Eng Chem Res 59:6347–6374
28. Sharma M, Gaur A (2020) Photoinduced charge transfer in donor-bridge-acceptor in one- and two-photon absorption: sequential and superexchange mechanisms. J Phys Chem C 124:4927–4930
29. Abdah MAAM, Azman NHN, Kulandaivalu S, Sulaiman Y (2020) Review of the use of transition-metal-oxide and conducting polymer-based fibres for high-performance supercapacitors. Mater Design 186:108199
30. Yu L, Chen CZ (2020) Supercapatteries as high-performance electrochemical energy storage devices. Electrochem Energy Rev 3:271–285
31. Samy MM, Mohamed MG, Kuo SW (2020) Directly synthesized nitrogen-and-oxygen–doped microporous carbons derived from a bio-derived polybenzoxazine exhibiting high-performance supercapacitance and CO_2 uptake. Eur Polym J 138:109954
32. Moussa M, El-Kady MF, Dubal D, Tung TT, Nine MJ, Mohamed N, Kaner RB, Losic D (2020) Self-assembly and cross-linking of conducting polymers into 3D hydrogel electrodes for supercapacitor applications. ACS Appl Energy Mater 3:923–932
33. El-Mahdy AFM, Yu TC, Mohamed MG, Kuo SW (2021) Secondary structures of polypeptide-based diblock copolymers influence the microphase separation of templates for the fabrication of microporous carbons. Macromolecules 54:1030–1042
34. Zhang LL, Zhao XS (2009) Carbon-based materials as supercapacitor electrodes. Chem Soc Rev 38:2520–2531
35. Vlad A, Singh N, Galande C, Ajayan P (2015) Design considerations for unconventional electrochemical energy storage architectures. Adv Energy Mater 5:1402115

36. Zhu YW, Murali S, Stoller MD, Ganesh KJ, Cai WW, Ferreira PJ, Pirkle A, Wallace RM, Cychosz KA, Thommes M, Su D, Stach EA, Ruoff RS (2011) Carbon-based supercapacitors produced by activation of graphene. Science 332:1537–1541
37. Wang Y, Shi ZQ, Huang Y, Ma YF, Wang CY, Chen MM, Chen YS (2009) Supercapacitor devices based on grapheme materials. J Phys Chem C 113:13103–13107
38. Liu C, Yu Z, Neff D, Zhamu A, Jang BZ (2010) Graphene-based supercapacitor with an ultrahigh energy density. Nano Lett 10:4863–4868
39. Miller J, Simon P (2008) Electrochemical capacitors for energy management. Science 321:651–652
40. El-Mahdy AFM, Zakaria MB, Wang HX, Chen T, Yamauchi Y, Kuo SW (2020) Heteroporous bifluorenylidene-based covalent organic frameworks displaying exceptional dye adsorption behavior and high energy storage. J Mater Chem A 8:25148–25155
41. Sang Y, Chen G, Huang J (2020) Oxygen-rich porous carbons from carbonyl modified hyper-cross-linked polymers for efficient CO_2 capture. J Polym Res 27:36
42. Mohamed MG, Lee CC, El-Mahdy AFM, Lüder J, Yu MH, Li Z, Zhu Z, Chueh CC, Kuo SW (2020) Exploitation of two-dimensional conjugated covalent organic frameworks based on tetraphenylethylene with bicarbazole and pyrene units and applications in perovskite solar cells. J Mater Chem A 8:11448–11459
43. Abuzeid HR, El-Mahdy AFM, Kuo SW (2021) Covalent organic frameworks: design principles, synthetic strategies, and diverse applications. Giant 6:100054
44. Mohamed MG, El-Mahdy AFM, Meng TS, Samy MM, Kuo SW (2020) Multifunctional hypercrosslinked porous organic polymers based on tetraphenylethene and triphenylamine derivatives for high-performance dye adsorption and supercapacitor. Polymers 12:2426
45. Cooper AI (2009) Conjugated microporous polymers. Adv Mater 21:1291–1295
46. Chaoui N, Trunk M, Dawson R, Schmidt J, Thomas A (2017) Trends and challenges for microporous polymers. Chem Soc Rev 46:3302–3321
47. Zhang X, Qiu B, Zou Y, Wang S, Mai W, Cao Y, Wang Y, Chen J, Li T (2020) Green synthesized cobalt-bipyridine constructed conjugated microporous polymer: An efficient heterogeneous catalyst for cycloaddition of epoxides via CO_2 fixation under ambient conditions. Micropor Mesopor Mat 319:110758
48. Aly KI, Sayed MM, Mohamed MG, Kuo SW, Younis O (2020) A facile synthetic route and dual function of network luminescent porous polyester and copolyester containing porphyrin moiety for metal ions sensor and dyes adsorption. Micropor. Mesopor. Mat. 298:110063.
49. Geng T, Zhang C, Chen G, Ma L, Zhang W, Xia H (2019) Synthesis of tetraphenylethylene-based fluorescent conjugated microporous polymers for fluorescent sensing and adsorbing iodine. Micropor Mesopor Mat 284:468–475
50. Mohamed MG, Elsayed MH, Elewa AM, EL-Mahdy AFM, Yang CH, Mohammed AAK, Chou HH, Kuo SW (2021) Pyrene-containing conjugated organic microporous polymers for photocatalytic hydrogen evolution from water. Catal Sci Technol 11:2229–2241
51. Mohamed MG, Ebrahium SM, Hammam AS, Kuo SW, Aly KI (2020) Enhanced CO_2 capture in nitrogen-enriched microporous carbons derived from Polybenzoxazines containing azobenzene and carboxylic acid units. J Polym Res 27:197
52. Dai C, Zhong L, Gong X, Zeng L, Xue C, Li S, Liu B (2019) Triphenylamine based conjugated microporous polymers for selective photoreduction of CO_2 to CO under visible light. Green Chem 2:6606–6610
53. Sprick RS, Bai Y, Guilbert AAY, Zbiri M, Aitchison CM, Wilbraham L, Yan Y, Woods DJ, Zwijnenburg MA, Cooper AI (2019) Photocatalytic hydrogen evolution from water using fluorene and dibenzothiophene sulfone-conjugated microporous and linear polymers. Chem Mater 2:305–313
54. Zhang C, He Y, Mu P, Wang X, He Q, Chen Y, Zeng J, Wang F, Xu Y, Jiang JX (2018) Toward high performance thiophene-containing conjugated microporous polymer anodes for lithium-ion batteries through structure design. Adv Funct Mater 28:1705432
55. Sprick RS, Jiang JX, Bonillo B, Ren S, Ratvijitvech T, Guiglion P, Zwijnenburg MA, Adams DJ, Cooper AI (2015) Tunable organic photocatalysts for visible-light-driven hydrogen evolution. J Am Chem Soc 137:3265–3270
56. Ma W, Zhang C, Gao X, Shu C, Yan C, Wang F, Chen Y, Zeng JH, Jiang JX (2020) Structure evolution of azo-fused conjugated microporous polymers for high performance lithium-ion batteries anodes. J Power Sources 453:227868
57. Zhang C, Qiao Y, Xiong P, Ma W, Bai P, Wang X, Li Q, Zhao J, Xu Y, Chen Y, Zeng JH, Wang F, Xu Y, Jiang JX (2019) Conjugated microporous polymers with tunable electronic structure for high-performance potassium-ion batteries. ACS Nano 13:745–754
58. Xu F, Chen X, Tang Z, Wu D, Fu R, Jiang D (2014) Redox-active conjugated microporous polymers: a new organic platform for highly efficient energy storage. Chem Commun 50:4788–4790
59. Jiang JX, Su F, Trewin A, Wood CD, Niu H, Jones JTA, Khimyak YZ, Cooper AI (2008) Synthetic control of the pore dimension and surface area in conjugated microporous polymer and copolymer networks. J Am Chem Soc 130:7710–7720
60. Jiang JX, Su F, Trewin A, Wood CD, Campbell NL, Niu H, Dickinson C, Ganin AY, Rosseinsky MJ, Khimyak YZ, Cooper AI (2007) Conjugated microporous poly(aryleneethynylene) networks. Angew Chem Int Ed 46:8574–8578
61. Zhang S, Huang W, Hu P, Huang C, Shang C, Zhang C, Yang R, Cui G (2015) Conjugated microporous polymers with excellent electrochemical performance for lithium and sodium storage. J Mater Chem A 3:1896–1901
62. Zhang C, Yang X, Ren W, Wang Y, Su F, Jiang JX (2016) Microporous organic polymer-based lithium ion batteries with improved rate performance and energy density. J Power Sources 317:49–56
63. Amin K, Ashraf N, Mao L, Faul CFJ, Wei Z (2021) Conjugated microporous polymers for energy storage: Recent progress and challenges. Nano Energy 85:105958
64. Wang HG, Cheng ZH, Liao YZ, Li JH, Weber J, Thomas A, Faul CFJ (2017) Conjugated microporous polycarbazole networks as precursors for nitrogen-enriched microporous carbons for co2 storage and electrochemical capacitors. Chem Mater 29:4885
65. Vilela F, Zhang K, Antonietti M (2012) Conjugated porous polymers for energy applications. Energy Environ Sci 5:7819–7832
66. Schmidt J, Weber J, Epping JD, Antonietti M, Thomas A (2009) Microporous conjugated poly(thienylene arylene) networks. Adv Mater 21:702–705
67. Lee JSM, Cooper AI (2020) Advances in conjugated microporous polymers. Chem Rev 120:2171–2214
68. Mohamed MG, Liu NY, EL-Mahdy AFM, Kuo SW (2021) Ultrastable luminescent hybrid microporous polymers based on polyhedral oligomeric silsesquioxane for CO_2 uptake and metal ion sensing. Micropor Mesopor Mat 311:110695
69. Mohamed MG, Kuo SW (2019) Functional polyimide/polyhedral oligomeric silsesquioxane nanocomposites. Polymers 11:26
70. Mohamed MG, Tsai MY, Wang CF, Huang CF, Danko M, Dai L, Chen T, Kuo SW (2021) Multifunctional polyhedral oligomeric silsesquioxane (poss) based hybrid porous materials for co2 uptake and iodine adsorption. Polymers 13:221
71. Zhang X, Zhao S, Kuo SW, Chen WC, Mohamed MG, Xin Z (2021) An effective nucleating agent for isotactic polypropylene (iPP): Zinc bis- (nadic anhydride) double-decker silsesquioxanes. Polymer 220:123574.

72. Liao YT, Lin YC, Kuo SW (2017) Highly thermally stable, transparent, and flexible polybenzoxazine nanocomposites by combination of double-decker-shaped polyhedral silsesquioxanes and polydimethylsiloxane. Macromolecules 50:5739–5747
73. Chen WC, Kuo SW (2018) Ortho-imide and allyl groups effect on highly thermally stable polybenzoxazine/double-decker-shaped polyhedral silsesquioxane hybrids. Macromolecules 51:9602–9612
74. Mohamed MG, Kuo SW (2019) Functional silica and carbon nanocomposites based on polybenzoxazines. Macromol Chem Phys 220:1800306
75. Zhang X, Zhao S, Mohamed MG, Kuo SW, Xin Z (2020) Crystallization behaviors of poly (ethylene terephthalate) (PET) with monosilane isobutyl-polyhedral oligomeric silsesquioxanes (POSS). J Mater Sci 55:14642–14655
76. Wang D, Yang W, Feng S, Liu H (2016) Amine post-functionalized POSS-based porous polymers exhibiting simultaneously enhanced porosity and carbon dioxide adsorption properties. RSC Adv 6:13749–13756
77. Wang D, Li L, Yang W, Zuo Y, Feng S, Liu H (2014) POSS-based luminescent porous polymers for carbon dioxide sorption and nitroaromatic explosives detection. RSC Adv 4:59877–59884
78. Sun L, Liang Z, Yu J (2015) Octavinylsilsesquioxane-based luminescent nanoporous inorganic–organic hybrid polymers constructed by the Heck coupling reaction. Polym Chem 6:917–924
79. Zhang L, Abbenhuis HCL, Yang Q, Wang YM, Magusin PCMM, Mezari B, van Santen RA, Li C (2007) Mesoporous organic–inorganic hybrid materials built using polyhedral oligomeric silsesquioxane blocks. Angew Chem Int Ed 46:5003–5006
80. Wang D, Yang W, Feng S, Liu H (2014) Constructing hybrid porous polymers from cubic octavinyl silsequioxane and planar halogenated benzene. Polym Chem 5:3634–3642
81. Chaikittisilp W, Sugawara A, Shimojima A, Okubo T (2010) Hybrid porous materials with high surface area derived from bromophenylethenyl-functionalized cubic siloxane-based building units. Chem Eur J 16:6006–6014
82. Liu XY, Zhang YL, Fei X, Liao LS, Fan J (2019) 9,9'-Bicarbazole: New Molecular Skeleton for Organic Light-Emitting Diodes. Chem Eur J 25:4501–4508
83. Yuan Y, Huang H, Chen L, Chen YY (2017) N, N'-Bicarbazole: A versatile building block toward the construction of conjugated porous polymers for CO_2 capture and dyes adsorption. Macromolecules 50:4993–5003
84. Chen WC, Ahmed MMM, Wang CF, Huang CF, Kuo SW (2019) Highly thermally stable mesoporous poly(cyanate ester) featuring double-decker–shaped polyhedral silsesquioxane framework. Polymer 185:121940
85. Wu JY, Mohamed MG, Kuo SW (2017) Directly synthesized nitrogen-doped microporous carbons from polybenzoxazine resins for carbon dioxide capture. Polym Chem 8:5481–5489
86. Singh G, Lee J, Karakoti A, Bahadur R, Yi J, Zhao D, AlBahily K, Vinu A (2020) Emerging trends in porous materials for CO_2 capture and conversion. Chem Soc Rev 49:4360–4404
87. Lashaki MJ, Khiavi S, Sayari A (2019) Stability of amine-functionalized CO_2 adsorbents: a multifaceted puzzle. Chem Soc Rev 48:3320–3405
88. DeBlase CR, Silberstein KE, Truong TT, Abruña HD, Dichtel WR (2013) β-Ketoenamine-linked covalent organic frameworks capable of pseudocapacitive energy storage. J Am Chem Soc 135:16821–16824
89. Mohamed MG, Zhang X, Mansoure TH, El-Mahdy AFM, Huang CF, Danko M, Xin Z, Kuo SW (2020) Hypercrosslinked porous organic polymers based on tetraphenylanthraquinone for CO_2 uptake and high-performance supercapacitor. Polymer 205:122857
90. El-Mahdy AFM, Young C, Kim J, You J, Yamauchi Y, Kuo SW (2019) Hollow microspherical and microtubular [3+3] carbazole-based covalent organic frameworks and their gas and energy storage applications. ACS Appl Mater Interfaces 11:9343–9354
91. El-Mahdy AFM, Kuo CH, Alshehri A, Young C, Yamauchi Y, Kim J, Kuo SW (2018) Strategic design of triphenylamine- and triphenyltriazine-based two-dimensional covalent organic frameworks for CO_2 uptake and energy storage. J Mater Chem A 6:19532–19541